Diagn Interv Radiol 2023; DOI: 10.4274/dir.2023.222006

MODALITY-BASED (UC, CT, MRI, PET-CT) IMAGING

ORIGINAL ARTICLE

Multivariate analysis based on the maximum standard unit value of ^{18}F-fluorodeoxyglucose positron emission tomography/computed tomography and computed tomography features for preoperative predicting of visceral pleural invasion in patients with subpleural clinical stage IA peripheral lung adenocarcinoma

Yun Wang†
Deng Lyu†
Taohu Zhou
Wenting Tu
Li Fan
Shiyuan Liu

†Yun Wang and Deng Lyu contributed equally to this work.

From the Department of Radiology (Y.W., D.L., W.T., L.F. ✉ fanli0930@163.com, S.L. ✉ radiology_cz@163.com), Second Affiliated Hospital of Navy Medical University, Shanghai, China; Department of Radiology (T.Z.), Weifang Medical University, School of Medical Imaging, Weifang, China.

Received 13 November 2022; revision requested 23 December 2022; last revision received 30 January 2023; accepted 02 February 2023.

Epub: 21.02.2023

Publication date: 29.03.2023

DOI: 10.4274/dir.2023.222006

PURPOSE

Preoperative prediction of visceral pleural invasion (VPI) is important because it enables thoracic surgeons to choose appropriate surgical plans. This study aimed to develop and validate a multivariate logistic regression model incorporating the maximum standardized uptake value (SUV_{max}) and valuable computed tomography (CT) signs for the non-invasive prediction of VPI status in subpleural clinical stage IA lung adenocarcinoma patients before surgery.

METHODS

A total of 140 patients with subpleural clinical stage IA peripheral lung adenocarcinoma were recruited and divided into a training set (n = 98) and a validation set (n = 42), according to the positron emission tomography/CT examination temporal sequence, with a 7:3 ratio. Next, VPI-positive and VPI-negative groups were formed based on the pathological results. In the training set, the clinical information, the SUV_{max}, the relationship between the tumor and the pleura, and the CT features were analyzed using univariate analysis. The variables with significant differences were included in the multivariate analysis to construct a prediction model. A nomogram based on multivariate analysis was developed, and its predictive performance was verified in the validation set.

RESULTS

The size of the solid component, the consolidation-to-tumor ratio, the solid component pleural contact length, the SUV_{max}, the density type, the pleural indentation, the spiculation, and the vascular convergence sign demonstrated significant differences between VPI-positive (n = 40) and VPI-negative (n = 58) cases on univariate analysis in the training set. A multivariate logistic regression model incorporated the SUV_{max} [odds ratio (OR): 1.753, $P = 0.002$], the solid component pleural contact length (OR: 1.101, $P = 0.034$), the pleural indentation (OR: 5.075, $P = 0.041$), and the vascular convergence sign (OR: 13.324, $P = 0.025$) as the best combination of predictors, which were all independent risk factors for VPI in the training group. The nomogram indicated promising discrimination, with an area under the curve value of 0.892 [95% confidence interval (CI), 0.813–0.946] in the training set and 0.885 (95% CI, 0.748–0.962) in the validation set. The calibration curve demonstrated that its predicted probabilities were in acceptable agreement with the actual probability. The decision curve analysis illustrated that the current nomogram would add more net benefit.

CONCLUSION

The nomogram integrating the SUV_{max} and the CT features could non-invasively predict VPI status before surgery in subpleural clinical stage IA lung adenocarcinoma patients.

KEYWORDS

Computed tomography, lung adenocarcinoma, nomogram, positron emission tomography, visceral pleural invasion

You may cite this article as: Wang Y, Lyu D, Zhou T, Tu W, Fan L, Liu S. Multivariate analysis based on the maximum standard unit value of ^{18}F-fluorodeoxyglucose positron emission tomography/computed tomography and computed tomography features for preoperative predicting of visceral pleural invasion in patients with subpleural clinical stage IA peripheral lung adenocarcinoma. *Diagn Interv Radiol.* 2023;29(2):379-389.

The Global Cancer Statistics 2020 estimate that lung cancer incidence is 11.4%, with lung cancer being the world's second most prevalent type of malignant tumor and leading cause of cancer death, with an estimated 1.8 million deaths (18%) worldwide in 2020.[1] Lung adenocarcinoma accounts for the largest proportion of non-small cell lung cancer (NSCLC).[1]

Visceral pleural invasion (VPI) in lung cancer is defined as a tumor that invades beyond the visceral pleural elastic layer (PL1) and exposes the pleural surface (PL2); it is one of the poor prognostic factors.[2] According to the eighth edition of the tumor-node-metastasis (TNM) staging criteria, when cT1N0M0 lung adenocarcinoma has pathologically positive VPI, the tumor (T) stage is upgraded from T1 to T2, and the TNM stage is upgraded from IA to IB.[2]

According to recent studies, lobectomy surgery results in a better prognosis and lower intrathoracic recurrence for patients with clinical T1 stage tumors (including T1a) and pathologically confirmed positive VPI.[3] For patients with T1-sized VPI-positive lung cancer, more extensive lymph node dissection rather than lymph node sampling is required.[4] However, the conventional intraoperative diagnosing of VPI is time-consuming and inexact, with a reported accuracy of 56.5%.[5] The gold standard for diagnosis still relies on postoperative elastic fiber staining to evaluate VPI,[2] but postoperative pathology cannot guide preoperative surgical planning. Therefore, if the VPI status can be accurately assessed using preoperative imaging methods, it may significantly impact the surgical plan.

Previous studies have explored using computed tomography (CT) findings to predict VPI status.[6-15] Subpleural lung adenocarcinoma presenting as pure ground-glass nodules (pGGNs) do not enter the visceral pleura due to their low invasiveness.[11-13] In addition, VPI-positive status is never observed in lung cancer without a relationship with the pleura.[13,14] However, it is challenging to accurately determine the VPI status of lung cancers related to the adjacent pleura on CT, such as pleural tags or those in direct contact with the pleura. Positive predictive values range from 44.1% to 56.4%, indicating that approximately half of the CT-based predictions are false positives.[15] Therefore, finding novel and quickly available methods to improve efficiency is critical.

^{18}F-fluorodeoxyglucose (^{18}F-FDG) positron emission tomography (PET)/CT can reflect the glucose metabolism, the morphological characteristics of the tumors, and the anatomical relationship between adjacent structures, which is of great value for the TNM staging of tumors.[16] Recent studies have indicated that ^{18}F-FDG PET/CT has high accuracy in predicting the invasiveness,[17] the lymph node metastasis,[18] and the spread through air spaces[19] of clinical T1 stage NSCLC before surgery. However, establishing and validating a multivariate logistic regression model incorporating the maximum standardized uptake value (SUV_{max}) and the relevant CT signs for predicting the VPI status of clinical stage IA lung adenocarcinoma, excluding pGGNs and tumors unrelated to the pleura, is rare. A nomogram is based on multivariate regression analysis, integrating multiple predictors to transform complex regression equations into visual graphics, making the results of the prediction model more readable and convenient for evaluating patients. Because a nomogram is intuitive and easy to understand, it has been widely used in preoperative nodal staging, predicting invasiveness, and giving a lung cancer prognosis.[20-22] Therefore, this study aims to explore whether tumor metabolism information and CT features could accurately predict VPI in clinical stage IA lung adenocarcinoma based on a nomogram.

Main points

- ^{18}F-fluorodeoxyglucose positron emission tomography/computed tomography is valuable in the non-invasive diagnosis of visceral pleural invasion (VPI) in subpleural clinical stage IA lung adenocarcinoma patients.
- The maximum standardized uptake value (SUV_{max}), the solid component pleural contact length, the pleural indentation, and the vascular convergence sign are independent predictors of VPI.
- A nomogram incorporating SUV_{max} and independent computed tomography features improves predictive performance.

Methods

This retrospective study was approved by the Shanghai Changzheng Hospital Ethical Review Board of the hospital (decision number: CZ-20210528-01). Due to the retrospective nature of this study, informed consent was waived.

Patients

Between February 2015 and June 2022, 328 patients with clinical stage IA lung adenocarcinoma who underwent ^{18}F-FDG PET/CT examination before surgery and surgical resection were recruited. The inclusion criteria were as follows: (i) tumors clinically diagnosed as clinical T1 stage with a tumor size smaller than 30 mm[23] and (ii) tumors without pathological lymph node or distant metastasis. The exclusion criteria were as follows: (i) postoperative pathological diagnosis of atypical adenomatous hyperplasia (n = 1) or adenocarcinoma in situ (n = 1); (ii) no report of VPI status (n = 20); (iii) pGGNs (n = 14); (iv) neither directly in contact with the pleural surface nor had pleural tags (n = 107); (v) the minimum distance between the lesion and the pleura (DLP) >10 mm (n = 24); (vi) had treatment prior to ^{18}F-FDG PET/CT examination (n = 5); (vii) had a surgery and an examination interval of longer than 14 days (n = 6); and (viii) poor image quality or incomplete clinical data (n = 10). A total of 140 patients were included in our research (Figure 1). The patients were classified into a training and validation set with a 7:3 ratio based on the PET/CT examination temporal sequence. The training set included 98 patients between February 2015 and January 2020; the temporal validation set comprised 42 patients between April 2020 and June 2022.

Equipment and parameters

Whole-body PET/CT tomography was performed using a Siemens Biograph Truepoint 64 PET/CT. The fasting blood glucose level of the patient was less than 10 mmol/L before the examination. After measuring the patient's body weight, the patient was given an intravenous injection of ^{18}F-FDG (Shanghai Atomic Kexing Pharmaceutical Co., Ltd.) 3.70–5.55 MBq/kg (0.10–0.15 mCi/kg) body weight with a radiochemical purity >95%, followed by a 300 mL water drink. The patient was instructed to lie down and rest for 60 min in a dark room. After emptying the bladder, the body scan ranged from the base of the skull to the middle of the femur, scanning 5–7 beds, 2–3 min/bed, with a reconstruction matrix of 192 × 192. The PET images were attenuated by CT images and reconstructed iteratively. The body CT scanning parameters were as follows: tube voltage 120 kV, tube current 160 mAs, scanning layer thickness 3.75 mm, reconstruction matrix 512 × 512, and pitch 0.8 s. The chest high-resolution computed tomography (HRCT) scan parameters were as follows: tube voltage 120 kV, tube current 150 mAs, scanning layer thickness 5 mm, reconstruction layer thickness and layer interval 1 mm, reconstruction matrix 512 × 512, and pitch

0.8 s. The lung window images were reconstructed by a high-resolution algorithm (B70f), and the mediastinal window images were reconstructed using a standard algorithm (B40f).

Clinical and pathological data collection

Patients' clinical data, including age, gender, smoking history, preoperative carcinoembryonic antigen (CEA) level, surgical type, histological subtype, and tumor location, were reviewed.

The resected tissues were stained with hematoxylin and eosin, and the pathological diagnoses were performed by two pathologists with at least 10 years of experience. The specific elastic fiber stain was performed if the VPI status could not be determined accurately. Additionally, VPI was classified as no pleural invasion beyond the elastic layer (PL0), tumor invasion beyond the elastic layer (PL1), and tumor invasion to the surface of the visceral pleura (PL2), with PL1 and PL2 indicating the presence of VPI.[2]

Image evaluation

The ^{18}F-FDG PET/CT images were imported into the software (RadiAnt DICOM Viewer 4.2.1, Medixant, Poland) and analyzed by two independent radiologists with seven years of experience who were blinded to the pathological information. The lung window [width: 1.500 Hounsfield scale (HU), level: −500 HU], mediastinal window (width: 300 HU, level: 50 HU), multiplanar reformation (MPR), and maximal intensity projection were used to analyze the lesion. For quantitative indicators, the average measurements of two independent radiologists were used as the final data. For qualitative analysis, disagreements were discussed until a consensus was reached.

First, the tumor density type was classified as solid or part solid. The tumor size (the longest length of the tumor, T) and the solid component size (the longest length of the consolidation part, C) were measured at the lung window on the MPR images, and the proportion of the consolidation part was calculated (C/T ratio, CTR).[24]

Second, the tumor–pleura relationship was classified as a pleural attachment (directly contacting the pleura) or pleural tags (without abutting the pleura). Pleural tags were defined as one or multiple high-density linear strands connecting the tumor margin and the pleura (Figures 2-4).[8] The minimum vertical DLP was measured on the MPR images at the lung window for tumors with pleural tags (Figures 5, 6).[6] The pleural indentation sign was defined as the deviation of the pleura from its original position due to tumor traction at the lung window, which can be observed in tumors with pleural tags or pleural attachment (Figures 2, 7).[14] The longest interface length of the whole tumor

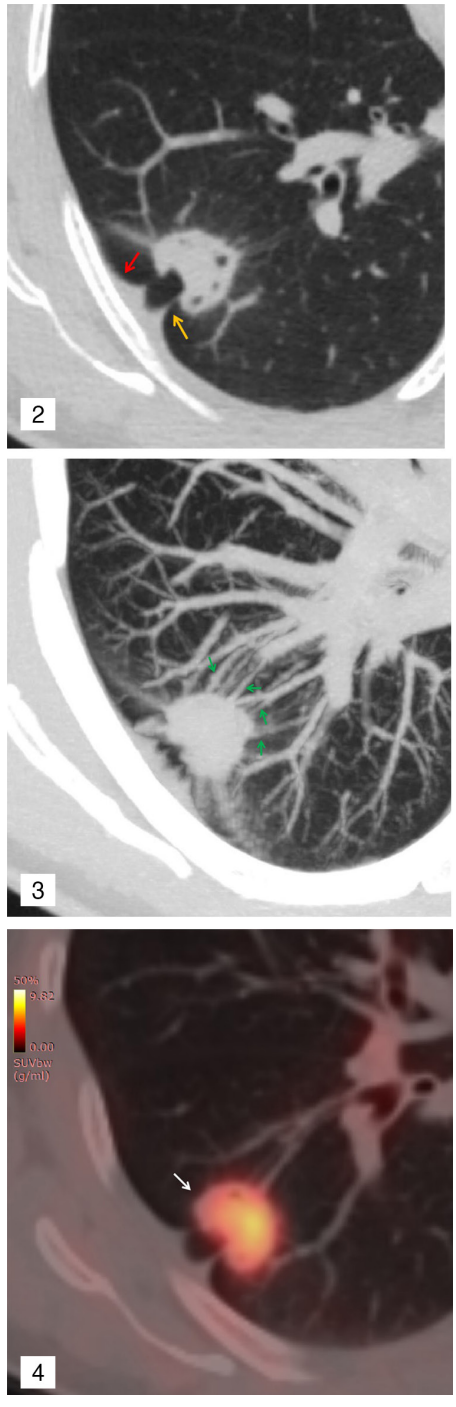

Figure 2-4. A 46-year-old female with invasive lung adenocarcinoma in the right lower lobe and positive for visceral pleural invasion. The axial non-contrast computed tomography **(Figure 2)** shows a solid nodule with multiple pleural tags (yellow arrow) and adjacent pleural indentation (red arrow). The maximal intensity projection **(Figure 3)** shows a vascular convergence sign (green arrow). The positron emission tomography/computed tomography fusion image **(Figure 4)** shows that the maximum standardized uptake value of the nodule is 6.38.

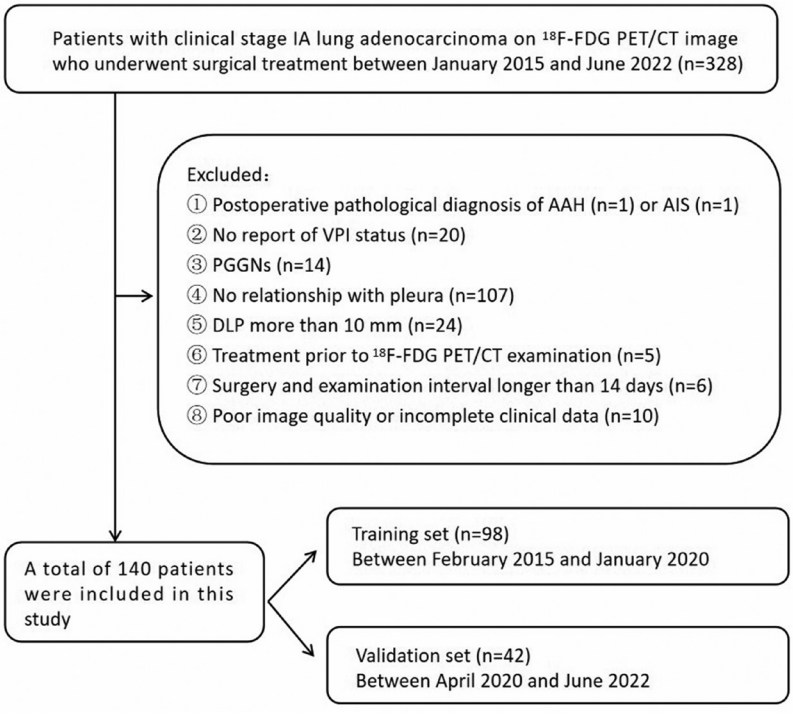

Figure 1. The flow chart for patient selection. AAH, atypical adenomatous hyperplasia; AIS, adenocarcinoma in situ; DLP, minimum distance between lesion and pleura; VPI, visceral pleural invasion; ^{18}F-FDG, ^{18}F-fluorodeoxyglucose; PET/CT, positron emission tomography/computed tomography; PGGN, pure ground-glass nodules.

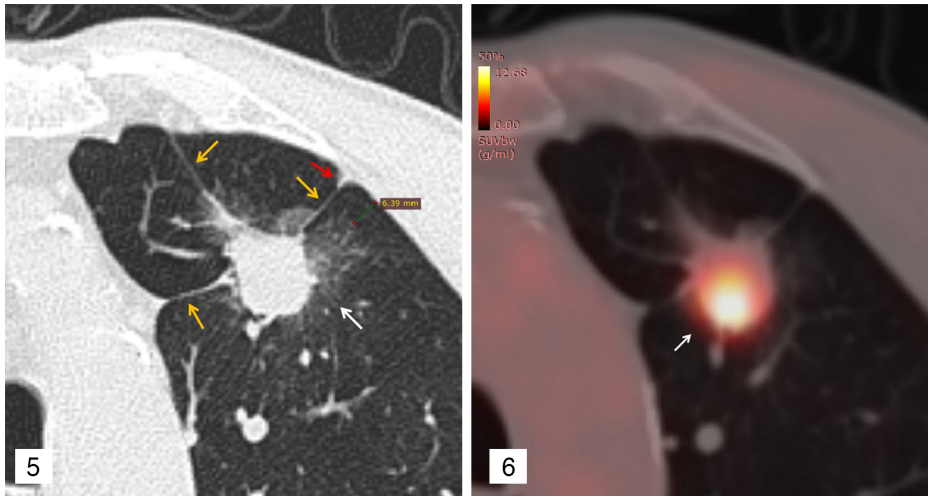

Figure 5, 6. A 72-year-old male with invasive lung adenocarcinoma in the left upper lobe and positive for visceral pleural invasion. The axial non-contrast computed tomography **(Figure 5)** shows a part-solid nodule with multiple pleural tags (yellow arrow) and adjacent pleural indentation (red arrow), with the minimum distance between the lesion and pleura being 6.39 mm. The positron emission tomography/computed tomography fusion image **(Figure 6)** shows that the uptake of ^{18}F-fluorodeoxyglucose is concentrated in the solid component area, and the maximum standardized uptake value of the nodule is 14.91.

and solid component was measured for tumors with pleural attachment by drawing a straight line at the lung window on the MPR images (Figure 7).[10] The solid interface length was 0 mm for a part-solid nodule without the solid component contacting the tumor.

Third, the presence or absence of lobulation, spiculation, vascular convergence, and air bronchogram signs were analyzed for all tumors. Lobulation is defined as a petaloid or wavy appearance at the tumor's margins. Spiculation refers to short, thin linear strands radiating around the surface of the tumor. Vascular convergence is the convergence of pulmonary vessels around the tumor towards the lesion (Figure 3).[22] Air bronchogram refers to air-filled bronchus manifesting as natural, dilated/distorted, or cut-off within the lesions.[25]

Fourth, the ^{18}F-FDG metric was measured by setting the region of interest covering the tumor on the PET/CT fusion images slice by slice and automatically generating the $SUV_{max.}$

Statistical analysis

R software (version 4.1.0, http://www.Rproject.org) and IBM SPSS Statistics (version 20.0, USA) software were utilized for the statistical analysis. The Shapiro–Wilk test was used to examine the normality of numeric variables. The normally distributed numerical variables were represented as the mean ± standard deviation, and the comparison between the two groups was carried out by using the two independent samples t-test. Non-normally distributed data were described as the median and the 25% and 75% quartiles, and the Mann–Whitney U test was performed. Pearson's chi-squared test or Fisher's exact test was used for categorical variables analysis. Variables significantly different ($P < 0.05$) in the univariate analysis were involved in the multivariate analysis of logistic regression, and a backward stepwise selection was applied by using the likelihood-ratio test with the Akaike information criterion (AIC) as the stopping rule to select the best combination of variables to build the prediction model in the training set and the corresponding nomogram. Spearman's rank correlation was used to analyze the correlation between the tumor size, the solid component size, the CTR, and the SUV_{max}. The interobserver agreement of numeric and categorical variables was assessed using the intraclass correlation coefficient (ICC) and κ-statistic, respectively. The receiver operating characteristic (ROC) curve with the corresponding area under the curve (AUC) value was used to evaluate the discrimination ability of the prediction model and each risk factor in predicting VPI in the training and validation set. The calibration curve and Hosmer–Lemeshow test were used to evaluate the goodness-of-fit of the prediction model, and a *P* value of greater than 0.05 indicated a good goodness-of-fit. The decision curve analysis (DCA) was used to evaluate the clinical utility of the nomogram. Multivariate binary logistic regression, nomogram, validation, and calibration plots were done with the "rms" package of R software. The ROC was performed by the "pROC" package, and the DCA was performed with the function of "ggDCA".

Results

Baseline characteristics of the study cohorts

Among the 140 clinical stage IA lung adenocarcinomas, 57 cases were VPI-positive, and 83 were VPI-negative. The baseline characteristics of the training and validation sets were similar ($P > 0.05$) (Table 1).

Clinical and ^{18}F-fluorodeoxyglucose positron emission tomography/computed tomography features by visceral pleural invasion status in the training group

Clinical features showed no significant differences in age ($P = 0.460$), gender ($P = 0.359$), tumor location ($P = 0.453$), smoking status ($P = 0.349$), and CEA level ($P = 1.000$) between the VPI-negative and VPI-positive groups in the training cohort (Table 2).

For ^{18}F-FDG PET/CT characteristics, the consistency of measurements between the two observers was good (ICCs ranged from 0.962 to 0.998), and the consistency of qualitative evaluation indicators was strong (a Kappa value of 0.879 to 0.971). The interobserver agreement assessment results of each index are shown in Supplementary File 1. The Spearman correlation analysis showed no linear correlation between the tumor size and the SUV_{max}. The solid component size was positively correlated with the SUV_{max} (r_s: 0.721, $P < 0.001$), while the CTR was positively correlated with the SUV_{max} (r_s: 0.742, $P < 0.001$). The univariate analysis showed that the SUV_{max}, the CTR, the solid component size, the solid pleural contact length, the density type, the pleural indentation, the spiculation, and the vascular convergence sign significantly differed between the VPI-positive and the VPI-negative groups in the training set ($P < 0.05$). The solid nodules, the pleural indentation, the spiculation, and the vascular convergence signs were more common in the VPI-positive group ($P < 0.001$). The VPI-positive group presented a significantly higher SUV_{max}, larger solid component size, greater CTR, and longer solid pleural contact length than the VPI-negative group ($P < 0.05$; Table 2).

Nomogram development and evaluation

Variables significantly different in the univariate analysis were involved in the multivariate logistic regression analysis. Based

Table 1. Baseline features of patients in the training and validation cohort

Characteristics	Total (n = 140)	Training cohort (n = 98)	Validation cohort (n = 42)	*P* value
Age[b]	60.50 ± 9.52	60.23 ± 9.51	61.12 ± 9.61	0.616
Gender				
Female	90 (64.29%)	64 (65.31%)	26 (61.90%)	0.700
Male	50 (35.71%)	34 (34.69%)	16 (38.10%)	
VPI status				
Negative	83 (59.29%)	58 (59.18%)	25 (59.52%)	0.970
Positive	57 (40.71%)	40 (40.82%)	17 (40.48%)	
Location[a]				
Right upper lobe	49 (35.00%)	34 (34.69%)	15 (35.71%)	
Right middle lobe	15 (10.71%)	9 (9.18%%)	6 (14.29%)	
Right lower lobe	28 (20.00%)	22 (22.45%)	6 (14.29%)	0.727
Left upper lobe	25 (17.85%)	18 (18.37%)	7 (16.67%)	
Left lower lobe	23 (16.44%)	15 (15.31%)	8 (19.04%)	
Smoking status				
Non smoker	112 (80.00%)	78 (79.59%)	34 (80.95%)	0.854
Smoker	28 (20.00%)	20 (20.41%)	8 (19.05%)	
CEA[a], μg/L				
<5	135 (96.43%)	96 (97.96%)	39 (92.86%)	0.159
≥5	5 (3.57%)	2 (2.04%)	3 (7.14%)	
Surgery type				
Sublobar resection	27 (19.29%)	18 (18.37%)	9 (21.43%)	0.674
Lobectomy	113 (80.71%)	80 (81.63%)	33 (78.57%)	
Pathological grade[a]				
MIA	4 (2.86%)	4 (4.08%)	0 (0.00%)	0.316
IA	136 (97.14%)	94 (95.92%)	42 (100.00%)	
SUV_{max}	1.84 (1.22, 3.78)	1.80 (1.04, 3.84)	1.88 (1.27, 3.53)	0.297
Tumor size (mm)	24.10 (19.20, 28.95)	23.80 (18.40, 28.70)	26.20 (20.40, 29.40)	0.193
Solid component size (mm)	17.15 (10.85, 23.35)	16.40 (9.67, 21.80)	19.00 (12.70, 26.70)	0.068
CTR (%)	78.14 (53.35, 95.98)	74.31 (47.51, 93.75)	83.76 (66.30, 100.00)	0.106
Pleural contact length (mm)	7.87 (0.00, 16.55)	7.24 (0.00, 15.80)	9.12 (0.00, 17.30)	0.612
Solid pleural contact length (mm)	2.84 (0.00, 10.65)	0.00 (0.00, 10.10)	4.40 (0.00, 13.80)	0.255
DLP (mm)	0.00 (0.00, 3.36)	0.00 (0.00, 3.50)	0.00 (0.00, 2.71)	0.467
Density type				
Part solid	108 (77.14%)	77 (78.57%)	31 (73.81%)	0.539
Solid	32 (22.86%)	21 (21.43%)	11 (26.19%)	
Tumor–pleura relationship				
Pleural tags	64 (45.71%)	45 (45.92%)	19 (45.24%)	0.941
Pleural attachment	76 (54.29%)	53 (54.08%)	23 (54.76%)	
Pleural indentation				
Absent	54 (38.57%)	34 (34.69%)	20 (47.62%)	0.150
Present	86 (61.43%)	64 (65.31%)	22 (52.38%)	
Lobulation[a]				
Absent	13 (9.29%)	11 (11.24%)	2 (4.76%)	0.344
Present	127 (90.71%)	87 (88.76%)	40 (95.24%)	
Spiculation				
Absent	105 (75.00%)	72 (73.47%)	33 (78.57%)	0.523
Present	35 (25.00%)	26 (26.53%)	9 (21.43%)	
Air bronchogram				
Absent	55 (39.29%)	41 (41.84%)	14 (33.33%)	0.345
Present	85 (60.71%)	57 (58.16%)	28 (66.67%)	
Vascular convergence				
Absent	116 (82.86%)	83 (84.69%)	33 (78.57%)	0.378
Present	24 (17.14%)	15 (15.31%)	9 (21.43%)	

The *P* value represents the univariate analysis. Data are presented as n (%). [a]Fisher exact test; [b]mean ± standard deviation, the two independent samples t-test. VPI, visceral pleural invasion; CEA, carcinoembryonic antigen; MIA, minimally invasive adenocarcinoma; IA, invasive adenocarcinoma; CTR, consolidation-to-tumor ratio; SUV_{max}, maximum standardized uptake value; DLP, minimum distance between lesion and pleura.

on the principle of AIC value minimization, a prediction model was constructed by a backward stepwise selection of variables, including the SUV_{max}, the solid component pleural contact length, the pleural indentation, and the vascular convergence sign as the best combination of prediction variables. The SUV_{max} [odds ratio (OR): 1.753, 95% confidence interval (CI) 1.232–2.496, P = 0.002], the solid component pleural contact length (OR: 1.101, 95% CI 1.007–1.204, P = 0.034), the pleural indentation (OR: 5.075, 95% CI 1.065–24.172, P = 0.041), and the vascular convergence sign (OR: 13.324, 95% CI 1.379–128.691, P = 0.025) were independent risk factors for VPI (Table 3). Figures 2 to 8 show the representative cases.

Based on the regression coefficients of the variables included in this model, a nomogram was constructed to evaluate the VPI risk intuitively (Figure 9). The sensitivity, specificity, accuracy, and the AUC for the prediction model in the training set were 82.5%, 79.31%, 80.61%, and 0.892 (95% CI 0.813–0.946), respectively, using the optimal cut-off value of 0.35. The prediction model achieved good discrimination performance in the validation set with sensitivity, specificity, accuracy, and AUC values of 100%, 76.00%, 85.71%, and 0.885 (95% CI, 0.748–0.962), respectively. Figures 10 and 11 present the ROCs for the training and validation cohorts. Table 4 shows the cut-off values and predictive performance of each independent risk factor for predicting VPI in the training and validation cohort. The calibration curve demonstrated that the predicted probabilities were in acceptable agreement with the actual probabilities for the training and validation cohorts, and the Hosmer–Lemeshow test showed good goodness of fit, with P values of 0.648 and 0.051, respectively (Figures 12, 13). The DCA showed that the prediction model adds more net benefit than the "treat all" or "treat none" approach (Figures 14, 15). Supplementary Figures 1, 2 give an example of the clinical application of this nomogram.

Discussion

The present study developed a prediction model as a non-invasive method to detect VPI status in clinical stage IA lung adenocarcinoma. The nomogram incorporating the SUV_{max}, the solid component pleural contact length, the pleural indentation, and the vascular convergence sign provided a scoring system to help predict VPI status before surgery and had excellent discrimination and acceptable calibration, with an AUC of 0.892 in the training set and 0.885 in the validation set.

The visceral pleura contains abundant lymphatic channels, and the subpleural lymphatic system (peripheral lymphatic system) communicates with the axial lymphatic system distributed around the bronchi and pulmonary vessels.[26] Therefore, lung cancer patients with VPI-positive status have a higher probability of hilar and mediastinal lymph node metastasis via the axial lymphatic system[27] and are more prone to skip N2 lymph node metastasis.[28] Thus, lobectomy and extensive lymph node dissection are required for VPI-positive patients.[3,4] Therefore, accurately predicting VPI before surgery is of great clinical significance.

For qualitative indicators, the present study found that the spiculation sign was more common in the VPI-positive group. Spiculation is associated with tumor cell infiltration into adjacent blood and lymphatic vessels, suggesting lung adenocarcinoma is more aggressive.[29] However, the spiculation sign was not an independent risk factor for VPI prediction in the present study, similar to the previous literature report.[30] As previously reported,[6,31] VPI was significantly related to the pleural indentation in the authors' study. The mechanism could be that as the tumor grows, the development of reactive fibrous hyperplasia of the tumor, to a certain extent, may cause the adjacent pleura to retract, thereby increasing the risk of VPI.[32] In addition to the pleural indentation sign, the vascular convergence sign was an independent risk factor in the present study, and no previous study reported similar results. It was speculated that it might be related to the pathological basis of the vascular convergence sign, which was also caused by the reactive fibrous hyperplasia of the tumor.[33] As tumor invasiveness increased, reactive fibrous hyperplasia increased, and traction

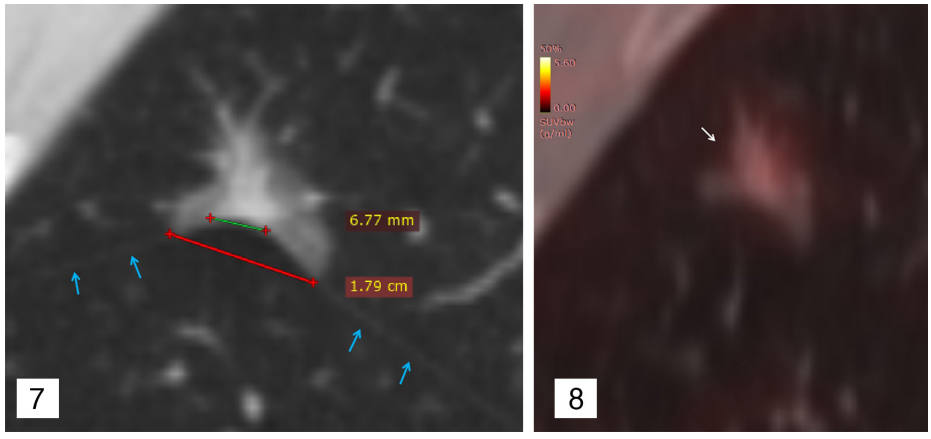

Figure 7, 8. A 61-year-old male with invasive lung adenocarcinoma in the right upper lobe and negative for visceral pleural invasion. The sagittal non-contrast computed tomography **(Figure 7)** shows a part-solid nodule with interlobar fissure attachment (blue arrow) and adjacent interlobar pleural indentation, with the longest interface length of the whole tumor and solid component being 1.79 cm and 6.77 mm, respectively. The image **(Figure 8)** shows the maximum standardized uptake value of the nodule is 0.95.

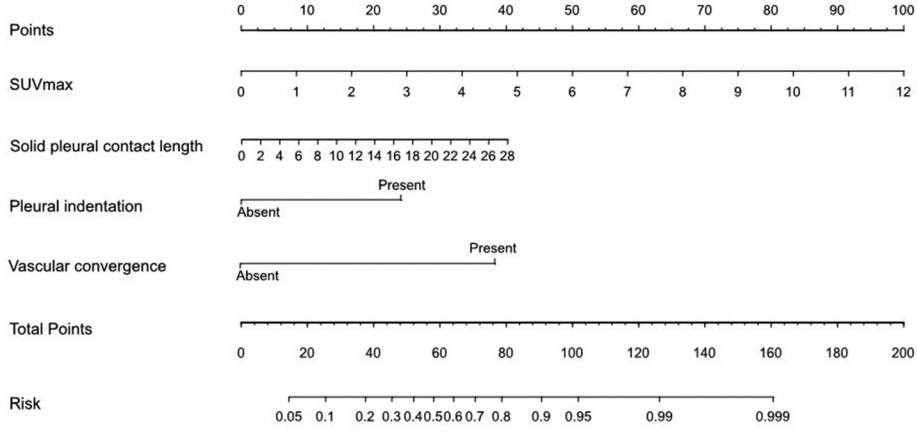

Figure 9. A ^{18}F-fluorodeoxyglucose positron emission tomography/computed tomography fusion nomogram for the non-invasive prediction of visceral pleural invasion for patients with clinical stage IA peripheral lung adenocarcinoma, which incorporated the maximum standardized uptake value, the solid component contact length, the pleural indentation, and the vascular convergence sign.

Table 2. Clinical characteristics and ^{18}F-fluorodeoxyglucose positron emission tomography/computed tomography features of patients in the training cohort

Characteristics	Total (n = 98)	VPI-negative (n = 58)	VPI-positive (n = 40)	*P* value
Age[b]	60.23 ± 9.51	60.83 ± 9.78	59.38 ± 9.16	0.460
Gender				
Female	64 (65.31%)	40 (68.97%)	24 (60.00%)	0.359
Male	34 (34.69%)	18 (31.03%)	16 (40.00%)	
Location[a]				
Right upper lobe	34 (34.69%)	17 (29.31%)	17 (42.50%)	
Right middle lobe	9 (9.18%)	4 (6.90%)	5 (12.5%)	
Right lower lobe	22 (22.45%)	14 (24.14%)	8 (20.00%)	0.453
Left upper lobe	18 (18.37%)	13 (22.41%)	5 (12.5%)	
Left lower lobe	15 (15.31%)	10 (17.24%)	5 (12.5%)	
Smoking status				
Non smoker	78 (79.59%)	48 (82.76%)	30 (75.00%)	0.349
Smoker	20 (20.41%)	10 (17.24%)	10 (25.00%)	
CEA[a]**, μg/L**				
<5	96 (97.96%)	57 (98.28%)	39 (97.50%)	1.000
≥5	2 (2.04%)	1 (1.72%)	1 (2.50%)	
SUV_{max}	1.80 (1.04, 3.84)	1.28 (0.86, 1.99)	3.36 (1.97, 6.23)	<0.001
Tumor size (mm)	23.80 (18.40, 28.70)	23.85 (17.50, 28.60)	23.75 (19.60, 28.90)	0.513
Solid component size (mm)[b]	16.09 ± 7.63	13.58 ± 7.43	19.75 ± 6.41	<0.001
CTR (%)	74.31 (47.51, 93.75)	63.90 (37.14, 76.17)	92.08 (77.71, 100.00)	<0.001
Pleural contact length (mm)	7.24 (0.00, 15.80)	3.35 (0.00, 15.50)	9.90 (0.00, 17.65)	0.301
Solid pleural contact length (mm)	0.00 (0.00, 10.10)	0.00 (0.00, 6.69)	5.77 (0.00, 16.75)	0.009
DLP (mm)	0.00 (0.00, 3.50)	0.56 (0.00, 3.57)	0.00 (0.00, 3.38)	0.547
Density type				
Part solid	77 (78.57%)	53 (91.38%)	24 (60.00%)	<0.001
Solid	21 (21.43%)	5 (8.62%)	16 (40.00%)	
Tumor-pleura relationship				
Pleural tags	45 (45.92%)	29 (50.00%)	16 (40.00%)	0.329
Pleural attachment	53 (54.08%)	29 (50.00%)	24 (60.00%)	
Pleural indentation				
Absent	34 (34.69%)	30 (51.72%)	4 (10.00%)	<0.001
Present	64 (65.31%)	28 (48.28%)	36 (90.00%)	
Lobulation[a]				
Absent	11 (11.22%)	7 (12.07%)	4 (10.00%)	1.000
Present	87 (88.78%)	51 (87.93%)	36 (90.00%)	
Spiculation				
Absent	72 (73.47%)	51 (87.93%)	21 (52.50%)	<0.001
Present	26 (26.53%)	7 (12.07%)	19 (47.50%)	
Air bronchogram				
Absent	41 (41.84%)	26 (44.83%)	15 (37.50%)	0.470
Present	57 (58.16%)	32 (55.17%)	25 (62.50%)	
Vascular convergence				
Absent	83 (84.69%)	57 (98.28%)	26 (65.00%)	<0.001
Present	15 (15.31%)	1 (1.72%)	14 (35.00%)	

The *P* value represents the univariate analysis. Data are presented as n (%). [a]Fisher exact test. [b]mean ± standard deviation, the two independent samples t-test. VPI, visceral pleural invasion; CEA, carcino-embryonic antigen; CTR, consolidation-to-tumor ratio; SUV_{max}, maximum standardized uptake value; DLP, minimum distance between lesion and pleura.

on adjacent pulmonary vessels or the pleura became more obvious.

For quantitative indicators, there was no linear correlation between the tumor size and the SUV_{max}, according to the Spearman correlation analysis, while the solid component size and the CTR had a relatively high degree of positive correlation with the SUV_{max}. This may be related to the larger proportion of part-solid nodules (78.57%) in the training set included in the present study. The tumor cells in the solid component area of the part-solid nodules were denser than in the ground glass area, so the ^{18}F-FDG uptake value was greater in the solid component area. Additionally, the SUV_{max}, the solid component size, the CTR, and the solid pleural contact length were significantly greater in the VPI-positive group ($P < 0.05$) than in the VPI-negative group, but the tumor size and the whole tumor pleural contact length did not show a difference between the two groups. The results indicate that the solid component represents the more aggressive part of the tumor, consistent with clinical T staging depending on the solid component's size rather than the tumor's overall size, in tumors less than 3 cm.[23] In this study, the analysis found that the SUV_{max} and the solid pleural contact length were independent risk factors for predicting VPI among quantitative indicators, similar to previous studies.[34,35] This result suggests that whether a solid component contacts the pleura and its contact length should also be an important consideration when determining VPI status. However, solid components in tumors may also correspond to fibroblast proliferation, alveolar collapse, inflammatory cell infiltration, and tumor-secreted mucus.[36] In some cases in the authors' study, although the solid component accounted for a large proportion, the SUV_{max} value was low, and the adjacent visceral pleura was not invaded (Supplementary Figures 1 to 2). Therefore, diagnostic efficacy for VPI status is limited when only considering the solid component size and the CTR. The SUV_{max} reflected the ^{18}F-FDG metabolism of tumors, representing the activity of tumor cell proliferation, and was a better indicator of tumor invasiveness in previous studies.[16-19] Furthermore, previous results found no VPI-positive status in clinical IA lung adenocarcinoma with the SUV_{max} less than 1.3,[34] indicating that an extremely low SUV_{max} can represent less invasiveness, which has a high negative predictive value.[34] Similar to the previous study, the authors' results also found that VPI-positive status was not observed in patients with an SUV_{max} of less than 1.4 in the training group. However, contrary to previous reports,[6,30] there was no significant difference in the DLP between the two groups. This may be because the proportion of tumors directly in contact with the pleura (pleura attachment) included in this study was comparable between the VPI-positive and VPI-negative groups in the training set, while the type of tumors in direct contact with the pleura (DLP = 0 mm) was more prevalent in the VPI-positive group in previous studies.[6,30] The different results are due to selection bias, and further verification is required after collecting large sample cases in the future.

There were two previous studies on predicting VPI status in lung adenocarcinoma based on ^{18}F-FDG PET/CT, but both of them only analyzed the risk factors related to VPI-positive status and did not validate the model. Tanaka et al.[34] studied the value of HRCT and ^{18}F-FDG PET/CT in predicting the pleural invasion of lung adenocarcinoma in direct contact with the pleura. In the subgroup analysis, including whole tumors size less than 3 cm, the multivariate analysis showed that the SUV_{max} and the whole tumor contact length with the pleura were independent risk factors for predicting pleural invasion. The predictive performance of only the SUV_{max} (AUC value 0.844) was comparable to the multivariate model (AUC value 0.845–0.857). Unlike the present study, the previous study included pGGNs and 11 cases with pathological parietal pleural invasion. The study by Chen et al.[35] focused on subsol-

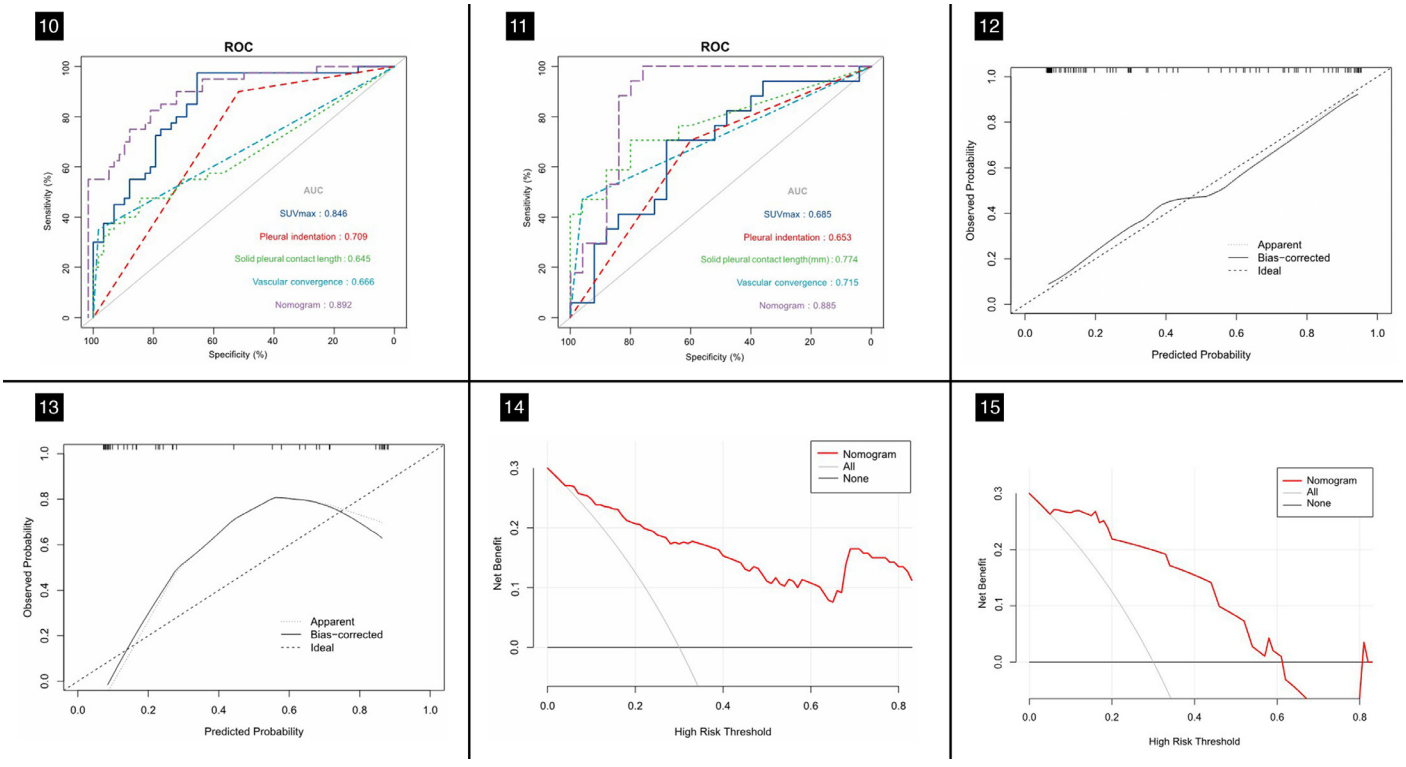

Figure 10-15. Receiver operating characteristic curves for the nomogram in the training set **(Figure 10)** and the validation set **(Figure 11)**. Calibration curves of the nomogram in the training set **(Figure 12)** and the validation set **(Figure 13)**. Decision curve analysis of the nomogram in the training set **(Figure 14)** and the validation set **(Figure 15)**.

id nodules, including pGGNs, and the multivariate analysis revealed that the DLP and the SUV_{max} were independent risk factors for predicting VPI. The AUC value of the combined model, including the two variables, was 0.90. However, Chen et al.[35] did not indicate whether the tumors included were related to the pleura, especially in the VPI-negative group. The present study excluded tumors presenting as pGGNs and tumors unrelated to the pleura that do not invade the visceral pleura, unlike in previous reports.[11-13] Therefore, the authors' results were more objective in including cases with potential VPI-positive status to study the predictive performance of the SUV_{max} combined with the CT features. The different results may be due to the different inclusion criteria of the study.

A previous study showed that ^{18}F-FDG liver metrics (the SUV_{max} and the SUV_{mean}) obtained from PET/CT studies of the same patient scanned on the same machine at different time periods were highly repeatable and might reliably be used in following patients longitudinally.[37] The SUV_{max} values in the present study were all obtained from a single ^{18}F-FDG PET/CT device in the same hospital; standardized image acquisition and post-processing were adopted, avoiding the differences brought by the hardware and post-processing software of the PET/CT equipment. It is worth noting that standardized image acquisition and post-processing of ^{18}F-FDG PET/CT and accurate measurement of the SUV_{max} are key factors in the preoperative assessment of whether lung cancer has invaded the visceral pleura.

This study has several limitations. First, the study was retrospective, resulting in inevitable selection bias. Second, although internal validation of the model yielded good discrimination, the generalization of this nomogram needs to be verified on external data. Third, VPI status in some cases lacks clear PL1 and PL2 pathological grades. Therefore, the clinical application and generalization of the model still need to be further improved and validated by multicenter studies.

In conclusion, the nomogram incorporating the SUV_{max} and the independent CT features (including the solid component pleural contact length, the pleural indentation, and the vascular convergence sign) showed good value for predicting VPI status in clinical stage IA lung adenocarcinoma in this preliminary study. As a non-invasive quantitative method, ^{18}F-FDG PET/CT holds the potential to help in the surgical decision-making process and additional treatment of clinical stage IA lung adenocarcinoma.

Acknowledgements

The authors thank Dr. Zhengwei Zhang of the Department of Pathology, Second Affiliated Hospital of Navy Medical University, Shanghai 200003, China, for his selfless and valuable assistance in interpreting the pathological results of this study.

Conflict of interest disclosure

The authors declared no conflicts of interest.

Funding

This research was funded by National Key R&D Program of China (2022YFC2010000, 2022YFC2010002), Key Program of National Natural Science Foundation of China (81930049), National Natural Science Foundation of China (82171926, 82202140), Shanghai Sailing Program (20YF1449000), Shanghai Science and Technology Innovation Action Plan Program (19411951300), Clinical Innovative Project of Shanghai Changzheng Hospital (2020YLCYJ-Y24), Program of Science and Technology Commission of Shanghai Municipality (21DZ2202600).

Table 3. Multivariate logistic regression analysis of independent risk factors for predicting visceral pleural invasion status in the training cohort

Characteristics	B	SE	Wald	*P* value	OR (95% CI)
SUV_{max}	0.562	0.180	9.711	0.002	1.753 (1.232–2.496)
Solid pleural contact length	0.097	0.046	4.491	0.034	1.101 (1.007–1.204)
Pleural indentation	1.624	0.796	4.159	0.041	5.075 (1.065–24.172)
Vascular convergence	2.590	1.157	5.008	0.025	13.324 (1.379–128.691)
Constant	–3.915	0.875	20.033	0.000	0.020

B, regression coefficients; SE, standard error; Wald, Wald χ^2 value; OR, odds ratio; CI, confidence interval; SUV_{max}, maximum standardized uptake value.

Table 4. The predictive efficacy of nomogram and single predictive factor for predicting visceral pleural invasion

Variable	Cut-off	Cohort	AUC (95% CI)	Accuracy (%)	Sensitivity (%)	Specificity (%)
Nomogram	0.35	Training	0.892 (0.813–0.946)	80.61	82.50	79.31
		Validation	0.885 (0.748–0.962)	85.71	100.00	76.00
SUV_{max}	1.43	Training	0.846 (0.759–0.911)	78.57	97.50	65.52
		Validation	0.685 (0.523–0.819)	69.05	70.59	68.00
Solid pleural contact length (mm)	8.92	Training	0.645 (0.542–0.739)	69.39	47.50	84.48
		Validation	0.744 (0.619–0.889)	76.19	70.59	80.00
Pleural indentation	0.50	Training	0.709 (0.608–0.796)	67.35	90.00	51.72
		Validation	0.653 (0.490–0.793)	64.29	70.59	60.00
Vascular convergence	0.50	Training	0.666 (0.564–0.758)	72.45	35.00	98.28
		Validation	0.715 (0.555–0.844)	76.19	47.06	96.00

SUV_{max}, maximum standardized uptake value; AUC, area under the curve; CI, confidence interval.

References

1. Sung H, Ferlay J, Siegel RL, et al. Global Cancer Statistics 2020: GLOBOCAN estimates of incidence and mortality worldwide for 36 cancers in 185 countries. *CA Cancer J Clin*. 2021;71(3):209-249. [CrossRef]
2. Goldstraw P, Chansky K, Crowley J, et al. The IASLC lung cancer staging project: proposals for revision of the TNM stage groupings in the forthcoming (Eighth) edition of the TNM classification for lung cancer. *J Thorac Oncol*. 2016;11(1):39-51. [CrossRef]
3. Zhang T, Zhang JT, Li WF, et al. Visceral pleural invasion in T1 tumors (≤3 cm), particularly T1a, in the eighth tumor-node-metastasis classification system for non-small cell lung cancer: a population-based study. *J Thorac Dis*. 2019;11(7):2754-2762. [CrossRef]
4. Wo Y, Zhao Y, Qiu T, et al. Impact of visceral pleural invasion on the association of extent of lymphadenectomy and survival in stage I non-small cell lung cancer. *Cancer Med*. 2019;8(2):669-678. [CrossRef]
5. Takizawa H, Kondo K, Kawakita N, et al. Autofluorescence for the diagnosis of visceral pleural invasion in non-small-cell lung cancer. *Eur J Cardiothorac Surg*. 2018;53(5):987-992. [CrossRef]
6. Qi LP, Li XT, Yang Y, et al. Multivariate analysis of pleural invasion of peripheral non-small cell lung cancer-based computed tomography features. *J Comput Assist Tomogr*. 2016;40(5):757-762. [CrossRef]
7. Yang S, Yang L, Teng L, et al. Visceral pleural invasion by pulmonary adenocarcinoma ≤3 cm: the pathological correlation with pleural signs on computed tomography. *J Thorac Dis*. 2018;10(7):3992-3999. [CrossRef]
8. Hsu JS, Han IT, Tsai TH, et al. Pleural tags on CT scans to predict visceral pleural invasion of non-small cell lung cancer that does not abut the pleura. *Radiology*. 2016;279(2):590-596. [CrossRef]
9. Onoda H, Higashi M, Murakami T, et al. Correlation between pleural tags on CT and visceral pleural invasion of peripheral lung cancer that does not appear touching the pleural surface. *Eur Radiol*. 2021;31(12):9022-9029. [CrossRef]
10. Heidinger BH, Schwarz-Nemec U, Anderson KR, et al. Visceral pleural invasion in pulmonary adenocarcinoma: differences in CT patterns between solid and subsolid cancers. *Radiol Cardiothorac Imaging*. 2019;1(3):e190071. [CrossRef]
11. Ahn SY, Park CM, Jeon YK, et al. Predictive CT features of visceral pleural invasion by T1-sized peripheral pulmonary adenocarcinomas manifesting as subsolid nodules. *AJR Am J Roentgenol*. 2017;209(3):561-566. [CrossRef]
12. Zhao Q, Wang JW, Yang L, Xue LY, Lu WW. CT diagnosis of pleural and stromal invasion in malignant subpleural pure ground-glass nodules: an exploratory study. *Eur Radiol*. 2019;29(1):279-286. [CrossRef]
13. Shi J, Li F, Yang F, et al. The combination of computed tomography features and circulating tumor cells increases the surgical prediction of visceral pleural invasion in clinical T1N0M0 lung adenocarcinoma. *Transl Lung Cancer Res*. 2021;10(11):4266-4280. [CrossRef]
14. Kim HJ, Cho JY, Lee YJ, et al. Clinical significance of pleural attachment and indentation of subsolid nodule lung cancer. *Cancer Res Treat*. 2019;51(4):1540-1548. [CrossRef]
15. Kim H, Goo JM, Kim YT, Park CM. CT-defined visceral pleural invasion in T1 Lung adenocarcinoma: lack of relationship to disease-free survival. *Radiology*. 2019;292(3):741-749. [CrossRef]
16. Kandathil A, Kay FU, Butt YM, Wachsmann JW, Subramaniam RM. Role of FDG PET/CT in the eighth edition of TNM staging of non-small cell lung cancer. *Radiographics*. 2018;38(7):2134-2149. [CrossRef]
17. Li XF, Shi YM, Niu R, et al. Risk analysis in peripheral clinical T1 non-small cell lung cancer correlations between tumor-to-blood standardized uptake ratio on 18F-FDG PET-CT and primary tumor pathological invasiveness: a real-world observational study. *Quant Imaging Med Surg*. 2022;12(1):159-171. [CrossRef]
18. Zhai X, Guo Y, Qian X. Combination of fluorine-18 fluorodeoxyglucose positron-emission tomography/computed tomography (^{18}F-FDG PET/CT) and tumor markers to diagnose lymph node metastasis in non-small cell lung cancer (NSCLC): a retrospective and prospective study. *Med Sci Monit*. 2020;26:e922675. [CrossRef]
19. Wang XY, Zhao YF, Yang L, Liu Y, Yang YK, Wu N. Correlation analysis between metabolic tumor burden measured by positron emission tomography/computed tomography and the 2015 World Health Organization classification of lung adenocarcinoma, with a risk prediction model of tumor spread through air spaces. *Transl Cancer Res*. 2020;9(10):6412-6422. [CrossRef]
20. Xie Y, Zhao H, Guo Y, et al. A PET/CT nomogram incorporating SUVmax and CT radiomics for preoperative nodal staging in non-small cell lung cancer. *Eur Radiol*. 2021;31(8):6030-6038. [CrossRef]
21. Jin C, Cao J, Cai Y, Wang L, Liu K, Shen W, Hu J. A nomogram for predicting the risk of invasive pulmonary adenocarcinoma for patients with solitary peripheral subsolid nodules. *J Thorac Cardiovasc Surg*. 2017;153(2):462-469. [CrossRef]
22. Song C, Guo Z, Yu D, et al. A prognostic nomogram combining immune-related gene signature and clinical factors predicts survival in patients with lung adenocarcinoma. *Front Oncol*. 2020;10:1300. [CrossRef]
23. Travis WD, Asamura H, Bankier AA, et al. The IASLC lung cancer staging project: proposals for coding T categories for subsolid nodules and assessment of tumor size in part-solid tumors in the forthcoming eighth edition of the TNM classification of lung cancer. *J Thorac Oncol*. 2016;11(8):1204-1223. [CrossRef]
24. Suzuki K, Koike T, Asakawa T, et al. A prospective radiological study of thin-section computed tomography to predict pathological noninvasiveness in peripheral clinical IA lung cancer (Japan Clinical Oncology Group 0201). *J Thorac Oncol*. 2011;6(4):751-756. [CrossRef]
25. Tu W, Sun G, Fan L, et al. Radiomics signature: a potential and incremental predictor for EGFR mutation status in NSCLC patients, comparison with CT morphology. *Lung Cancer*. 2019;132:28-35. [CrossRef]
26. Imai K, Minamiya Y, Saito H, et al. Detection of pleural lymph flow using indocyanine green fluorescence imaging in non-small cell lung cancer surgery: a preliminary study. *Surg Today*. 2013;43(3):249-254. [CrossRef]
27. Inoue M, Minami M, Shiono H, Sawabata N, Ideguchi K, Okumura M. Clinicopathologic study of resected, peripheral, small-sized, non-small cell lung cancer tumors of 2 cm or less in diameter: pleural invasion and increase of serum carcinoembryonic antigen level as predictors of nodal involvement. *J Thorac Cardiovasc Surg*. 2006;131(5):988-993. [CrossRef]
28. Gorai A, Sakao Y, Kuroda H, et al. The clinicopathological features associated with skip N2 metastases in patients with clinical stage IA non-small-cell lung cancer. *Eur J Cardiothorac Surg*. 2015;47(4):653-658. [CrossRef]
29. Jin C, Cao J, et al. A nomogram for predicting the risk of invasive pulmonary adenocarcinoma for patients with solitary peripheral subsolid nodules. *J Thorac Cardiovasc Surg*. 2017;153(2):462-469. [CrossRef]
30. Deng HY, Li G, Luo J, Alai G, Zhuo ZG, Lin YD. Novel biologic factors correlated to visceral pleural invasion in early-stage non-small cell lung cancer less than 3 cm. *J Thorac Dis*. 2018;10(4):2357-2364. [CrossRef]
31. Zhao LL, Xie HK, Zhang LP, et al. Visceral pleural invasion in lung adenocarcinoma ≤3 cm with ground-glass opacity: a clinical, pathological and radiological study. *J Thorac Dis*. 2016;8(7):1788-1797. [CrossRef]
32. Gruden JF. What is the significance of pleural tags? *AJR Am J Roentgenol*. 1995;164(2):503-504. [CrossRef]
33. Zhang Y, Qiang JW, Ye JD, Ye XD, Zhang J. High resolution CT in differentiating minimally invasive component in early lung adenocarcinoma. *Lung Cancer*. 2014;84(3):236-241. [CrossRef]
34. Tanaka T, Shinya T, Sato S, et al. Predicting pleural invasion using HRCT and 18F-FDG

PET/CT in lung adenocarcinoma with pleural contact. *Ann Nucl Med*. 2015;29(9):757-765. [CrossRef]

35. Chen Z, Jiang S, Li Z, Rao L, Zhang X. Clinical value of 18F-FDG PET/CT in prediction of visceral pleural invasion of subsolid nodule stage I lung adenocarcinoma. *Acad Radiol*. 2020;27(12):1691-1699. [CrossRef]
36. Park CM, Goo JM, Lee HJ, Lee CH, Chun EJ, Im JG. Nodular ground-glass opacity at thin-section CT: histologic correlation and evaluation of change at follow-up. *Radiographics*. 2007;27(2):391-408. [CrossRef]
37. Civelek A, Rana A, Malayeri et al. Intra and inter test reproducibility and comparison of PET-MRI and PET-CT derived 18F -FDG metric measurements. *J Nucl Med*. 2017;58(1):1343. [CrossRef]

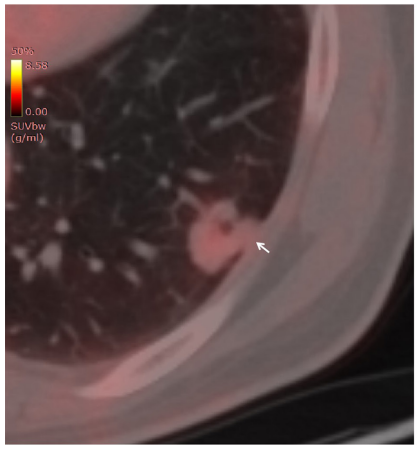

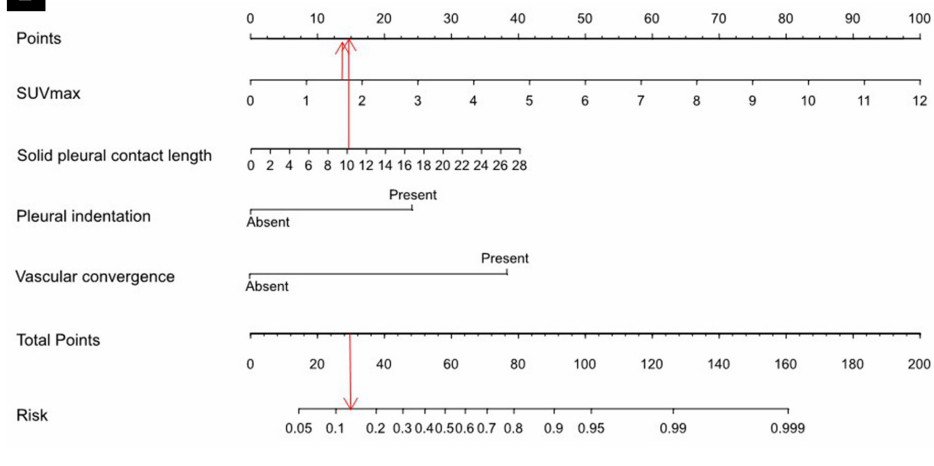

Supplementary Figures 1, 2. A 66-year-old male with invasive lung mucinous adenocarcinoma in the left lower lobe and negative for visceral pleural invasion. The positron emission tomography/computed tomography fusion image shows a solid nodule with pleural attachment (white arrow), without adjacent pleural indentation and vascular convergence, the solid component pleural contact length is 10.1 mm, and the maximum standardized uptake value of the nodule is 1.68 (**Supplementary Figure 1**). An example of the nomogram in clinical application (**Supplementary Figure 2**).

Supplementary file 1

Observer agreement

Methods

The strengths of the relation between the two sets of measurements were assessed with intraclass-correlation coefficients (ICC). Observer agreement for the assessment of tumor-pleura relationship, pleural indention, density type, lobulation, spiculation, air bronchogram and vascular convergence sign was calculated and evaluated using κ-statistics.

Results

The relation between the two sets of measurements was strong for maximum standardized uptake value [ICC: 0.987, 95% confidence interval (CI) 0.970 ~ 0.994, $P < 0.001$], tumor size (ICC: 0.970, 95% CI 0.958 ~ 0.978, $P < 0.001$), solid component size (ICC: 0.963, 95% CI 0.949 ~ 0.973), minimum distance between lesion and pleura (ICC: 0.962, 95% CI 0.948 ~ 0.973), pleural contact length (ICC: 0.996, 95% CI 0.995 ~ 0.997) and solid pleural contact length (ICC: 0.998, 95% CI 0.997 ~ 0.998). Observer agreement for assessment of tumor-pleura relationship, pleural indention, density type, lobulation, spiculation, air bronchogram and vascular convergence sign was excellent, with kappa values were 0.971, 0.879, 0.940, 0.877, 0.925, 0.955, 0.921, respectively.